Nanoscale

MINIREVIEW

View Article Online
View Journal | View Issue

Check for updates

Cite this: *Nanoscale*, 2018, **10**, 1570

Photodynamic therapy in 3D cancer models and the utilisation of nanodelivery systems

Layla Mohammad-Hadi, * Alexander J. MacRobert, Marilena Loizidou and Elnaz Yaghini *

Received 17th October 2017,
Accepted 15th December 2017

DOI: 10.1039/c7nr07739d

rsc.li/nanoscale

Photodynamic therapy (PDT) is the subject of considerable research in experimental cancer models mainly for the treatment of solid cancerous tumours. Recent studies on the use of nanoparticles as photosensitiser carriers have demonstrated improved PDT efficacy in experimental cancer therapy. Experiments typically employ conventional monolayer cell culture but there is increasing interest in testing PDT using three dimensional (3D) cancer models. 3D cancer models can better mimic *in vivo* models than 2D cultures by for example enabling cancer cell interactions with a surrounding extracellular matrix which should enable the treatment to be optimised prior to *in vivo* studies. The aim of this review is to discuss recent research using PDT in different types of 3D cancer models, from spheroids to nanofibrous scaffolds, using a range of photosensitisers on their own or incorporated in nanoparticles and nanodelivery systems.

Open Access Article. Published on 08 2018. Downloaded on 09-08-2025 20:27:54.
This article is licensed under a Creative Commons Attribution 3.0 Unported Licence.

Introduction

Photodynamic therapy (PDT) is a minimally invasive treatment for various cancers and for certain non-malignant lesions.[1] PDT requires administration of a photosensitiser, which is then activated by blue, red or near infrared (NIR) light resulting in the generation of cytotoxic reactive oxygen species (ROS). This method is clinically approved for treating several types of solid cancerous tumours for example prostate,[2] head and neck skin and oesophagus.[3] PDT has also been utilised to tackle non-cancerous conditions such as age-related macular degeneration, atherosclerosis and bacterial infections.[4] PDT treatment is advantageous for both the patient and the clinician since it minimises the need for major surgery, reduces recovery periods, promotes good healing and conserves integrity and function of organs with relatively little risk of local

Division of Surgery and Interventional Science, Department of Nanotechnology, University College London, Royal Free Campus, Rowland Hill St, London NW3 2PE, UK. E-mail: layla.hadi.13@ucl.ac.uk, elnaz.yaghini@ucl.ac.uk

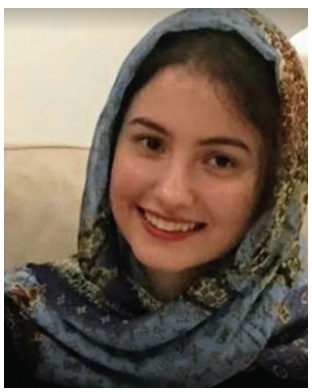

Layla Mohammad-Hadi

Layla Mohammad-Hadi is a doctoral student researching in nanomedicine and cancer therapy at University College London in the Dept. of Nanotechnology, Division of Surgery and Interventional Science. She graduated in Pharmacology and then completed a Masters degree in Reproductive Medicine and Women's Health. Her doctoral research is mainly focused on Photodynamic Therapy and the use of Photochemical internalisation for the delivery anti-cancer drugs to their target sites of action in various 3D models of breast and ovarian cancer.

Alexander J. MacRobert

Alexander (Sandy) MacRobert is a biophysical chemist and is Professor of Photochemistry and Photobiology at University College London. He was educated at the University of Cambridge and then carried out his PhD and postdoctoral research on free radical spectroscopy and kinetics in London at QMUL and Imperial College, Oxford University, and Bielefeld University, Germany. His research is focused on biomedical optical spectroscopy and imaging, and therapeutic applications of reactive oxygen species ranging from cancer to antimicrobial treatments.

This journal is © The Royal Society of Chemistry 2018

Open Access Article. Published on 08 2018. Downloaded on 09-08-2025 20:27:54.
This article is licensed under a Creative Commons Attribution 3.0 Unported Licence.

and systemic treatment-related morbidity and side-effects.[5–8] Furthermore PDT can be repeated and even used after various treatments such as surgery, chemotherapy and radiotherapy without inducing any immunosuppressive or myelosuppressive effects.[9]

Two dimensional (2D) cell culture where cells are grown on flat surfaces as monolayers and *in vivo* models have been the main means of conducting cancer and drug discovery studies until recently.[10] The 2D monolayer cultures present several advantages such as easy preparation, maintenance and monitoring in addition to being amenable for microscopic and molecular investigations.[11,12] However the growth of cells on a flat surface does not properly integrate important interactions between the cells and the surrounding extracellular matrix (ECM) that is present *in vivo* which consists largely of structural proteins, predominantly type 1 collagen fibrils.[13] Moreover cell-to-cell interaction is restricted in 2D models since the main interaction is with the host surface, normally plastic. The absence of such interactions in 2D models may cause adhesion properties and organization of cancer cells to deviate from their *in vivo* counterparts thereby affecting proliferation and signal transduction as well as cellular responses to drug and radiation therapies.[14,15] Moreover, when nanoparticles and drugs are applied to monolayer cell cultures they are able to reach cells without encountering any physical limitations whereas nanoparticles delivered *in vivo* experience hindrance by the ECM surrounding the cancer cells.[16] Thus exposure of the cancer cells in monolayer culture to a uniform environment with a steady supply of oxygen and nutrients prevents them from mimicking *in vivo* cancer tissues which are normally affected by nutrient and oxygen gradients[17] and can lead to altered gene expression patterns. The ECM is the major component of *in vivo* connective tissue,[18,19] and in solid tumours (*e.g.* colon, prostate, breast), the cancer cells grow and proliferate in contact with the surrounding connective tissue, which is also called the 'stroma'. The 3D models incorporating ECM materials such as collagen are therefore capable of mimicking cancer growth within its local environment, and provide a scaffold for cellular organisation in 3D and adoption of shape and structural features seen *in vivo*.[20–22] The stromal interactions exhibited in the 3D models can also influence therapeutic response,[23] drug and nanoparticle penetration, anti-apoptotic signalling as well as multicellular resistance and hypoxia.[16,24,25]

In this review we will be specifically discussing the use of PDT in different 3D cancer models with a focus on the possible application of nanoparticles in the PDT treatment of such models as seen in some of the studies mentioned later.

How PDT works

The mechanism of action of PDT and the nature of cell death depend on several factors such as genotype of cells, PDT dosimetry (*e.g.* light intensity) and the localisation of the photosensitiser.[26,27] Since most photosensitisers do not have the tendency to accumulate within the nuclei,[28] PDT rarely induces DNA related damage, mutations or carcinogenesis.[27] Photosensitisers, which localise within the mitochondria mainly, stimulate apoptosis,[29]whereas photosensitisers that localise within the plasma membrane mostly induce necrosis upon exposure to light.[30] Overall the manner in which cell death is triggered shifts from apoptotic to necrotic as the intensity of the damage caused to the cell becomes excessive resulting in swift cell lysis instead of an orderly programmed type of cell death.[31] Photodamage may also result in a cytoprotective response termed autophagy.[32]

Marilena Loizidou

Marilena Loizidou is Professor of Cancer Nanotechnology and Deputy Director of the Division of Surgery and Interventional Science (SIS) at University College London. She graduated in Biochemistry from McMasters University, Canada followed by a PhD in Solid Tumour Biology from the University of Southampton. She became lead clinical scientist at the University of Southampton/NHS and moved to UCL in 1993 becoming Head of Department at the Royal Free Campus in 2013. Her research focuses on targeting cancer using tissue engineered 3D in vitro *models of cancer from patient derived cells to determine responses to specific treatments.*

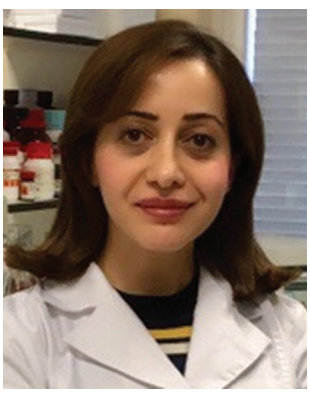

Elnaz Yaghini

Elnaz Yaghini is a senior research associate in the Division of Surgery and Interventional Science at University College London (UCL), and a member of the UCL Institute for Healthcare Engineering. She graduated in Clinical Medicine from Iran, followed by a PhD in Nanomedicine from UCL in 2011. In her research at UCL, she has investigated the potential of various nanoparticles and photosensitising dye molecules for preclinical diagnosis and treatment of cancer, and photochemical internalisation including the application of 3D models. Her research is primarily focused on the development of novel targeted fluorescent nanoparticles for cancer imaging and intraoperative image-guided surgery.

Open Access Article. Published on 08 2018. Downloaded on 09-08-2025 20:27:54.
This article is licensed under a Creative Commons Attribution 3.0 Unported Licence.

In terms of the photophysical processes involved in PDT, photosensitisers possess a stable singlet state as their lowest energy level[33] and upon light activation the photosensitiser is raised to a singlet excited state which is short-lived.[34,35] The photosensitiser may then return to ground state through internal conversion or radiatively *via* fluorescence which can be used for photodetection purposes in a clinical setting,[36] or be converted *via* intersystem crossing to the longer lived triplet state.[5] In this case, providing that a sufficient supply of oxygen is available, the excited triplet state photosensitiser can undergo either a type I or type II reaction process to produce ROS.[37] In a type I reaction the photosensitiser interacts with a substrate in a direct manner through proton or electron transfer to produce radicals.[38] In a type II reaction, resonant energy transfer occurs to generate the singlet oxygen species.[38] Due to the high reactivity and thus short diffusion distance of singlet oxygen, damage is locally confined,[39] and if the light field is well controlled, some selectivity of damage can be achieved to the target lesions with minimal damage occurring to the adjacent normal tissue.[38] However, singlet oxygen is still able to transverse and escape from inert matrices of nanocarriers such as mesoporous silica,[40] therefore photosensitisers incorporated within the nanoparticles can retain their photosensitisation properties, as discussed later. An extensive range of laser and non-laser sources of light can be used in photodynamic therapy.[41] Solid state semiconductor diode lasers provide cost-effective and high power delivery with the advantages of being portable and simple to operate.[42] Light delivery using optical fiber technology can either be directed onto the surface of the lesion using an endoscope or interstitially using multiple fibre-optic catheters implanted percutaneously within solid tumours.[43,44]

Photosensitisers used in PDT

An ideal photosensitiser should display chemical, photophysical as well as biological characteristics, which allow it to be taken up by tumours, undergo fast clearance and have a large absorption peak at red to near infrared wavelengths where tissue is relatively transparent.[39] Photosensitisers for PDT are normally categorised into two groups: tetrapyrrole derivatives (*e.g.* porphyrins) and non-tetrapyrroles (*e.g.* methylene blue).[27,45]

First and second-generation photosensitisers

First generation photosensitisers include haematoporphyrin derivatives (HpD) and a purified form of HpD known as porfimer sodium (Photofrin™). HpD has shown to localise within the tumours and produce a good tumouricidal response when activated by red light. Porfimer sodium has obtained FDA approval for treating lung and oesophageal using PDT.[46,47] Although porfimer sodium absorbs weakly around 630 nm,[47] it is still commonly used in clinical applications, however its more widespread use has been undermined by its retention in the skin resulting in long-term cutaneous photosensitivity.[5,48]

To address the limitations of these original photosensitisers, newer second-generation photosensitiers have been developed.[27] In comparison with the first generation agents, these photosensitisers are generally more chemically pure, capable of absorbing light at longer wavelengths, possess higher singlet oxygen quantum yields and induce lower skin photosensitivity.[39] The chlorin photosensitiser *m*-tetrahydroxyphenylchlorin (*m*THPC, temoporfin) is one of the most widely studied second-generation photosensitisers.[49] Another widely studied agent for PDT particularly in dermatology is 5-aminolaevulinic acid (ALA) which is a pro-drug for protoporphyrin IX (PPIX). However *m*THPC, has a higher potency than either of the porphyrin-based approaches using ALA,[39] or porfimer sodium[50] and requires lower light and drug doses for treating tumours.[51] Moreover *m*THPC absorbs light at 652 nm [52,53] in comparison to the weak absorption peak at 630 nm of both porfimer sodium and ALA induced PPIX which enables deeper excitation in the tissue.[53] For very thin lesions such as actinic keratoses in the skin, blue light excitation is sufficient and is used clinically with ALA. The search for drugs that are more tumour specific and can undergo activation with light of a longer wavelength with a shorter period of photosensitivity is still ongoing.[54] Other photosensitisers that have been tested in clinical trials include tin ethyl etiopurpurin (SnET2),[55] mono-L-aspartyl chlorin e6 (MACE),[56] benzoporphyrin derivative mono acid, ring A (BPD, verteporfin),[57] and lutetium texaphyrin (Lu-Tex).[58] These compounds have absorption peaks at higher wavelengths of 660 nm,[59] 664 nm,[56] 690 nm [60] and 732 nm respectively compared to first as well as second generation photosensitisers and lead to mild and brief skin photosensitivity. For clinical applications, a liposomal formulation (Visudyne™) of BPD is generally used.[61,62] The clinical formulation of *m*THPC is known as Foscan™. Liposomal formulations of *m*THPC have also been tested preclinically[49] known as Foslip™ and a pegylated version known as Fospeg™.

Description of different types of 3D cell culture models

3D culture models can be created using various formats such as multicellular aggregates, culturing cells on inserts or embedding cells in an artificial nanofibrous matrix or scaffold developed from natural or synthetic material.[63] The characteristics of different types of 3D models are summarised as follows.

Spheroids

Spheroids are well-rounded 3D cancer models typically several hundred μm in diameter that can also be referred to as spheres, nodules and micronodules.[64–66] Such 3D models can be created either by growing cells in low adhesion conditions

 This journal is © The Royal Society of Chemistry 2018

Open Access Article. Published on 08 2018. Downloaded on 09-08-2025 20:27:54.
This article is licensed under a Creative Commons Attribution 3.0 Unported Licence.

(*e.g.* plates, hanging drop methods *etc*.) where they assume naturally a spherical aggregate conformation[67–69] or by embedding cells in a 3D matrix. The closely packed arrangement where cell to cell contact is dominant and the reduced rate of diffusion of drugs and oxygen through the spheroids makes them comparable to *in vivo* tissues.[70] Spheroid 3D models are used for the assessment of various specific 3D properties such as the development of invasive characteristics, changes in the dependence of cells on growth factors, increased luminal survival because of the stimulation of anti-apoptotic and pro-proliferative signals and the capability to avoid growth arrest because of these pro-proliferative signals.[20,71] Spheroid 3D models have been widely used for a variety of photosensitiser-PDT studies including those involving two photon excitation (Table 1).

Cell derived matrices (CDMs)

CDMs are commonly produced by culturing cells that excrete ECM proteins on pre-coated scaffold surfaces or as a monolayer (2D), or multicellular aggregates (3D) to allow the deposition of adequate ECM. Upon depositing sufficient ECM, decellularisation processing can be used to disrupt as well as remove the cellular component from the ECM. Such processing is essential for minimising the risk of encountering adverse immunological responses.[72]

CDMs are known for providing a shared ECM based feedback to cancer cell signalling plus an enhanced cell–matrix adhesion, motility as well as proliferation compared to 2D cultures.[71] Such differences between CDMs and 2D cultures may arise due to expanded dimension or the activities of growth factors present in the CDMs, which are not detected in the 2D environments.[65,71] Moreover cells that are cultured on CDMs have similar morphologies to those observed *in vivo* since they can form specified 3D matrix adhesions, which are also found within *in vivo* models.[73]

Microfluidic devices

The microfluidic technology also known as Lab-on-a-chip (LOC)[74] provides the opportunity for the development of 3D cell cultures and cell based assays in complex microenvironments that can be controlled, reproduced and optimised.[75] This type of technology possesses several key features: (1) it exhibits micro-scale dimensions which have great compatibility to the microstructures found in the microenvironments of *in vivo* cancer models; (2) it is very cost-effective as a small quantity of the samples are required, keeping reagent consumption low thus reducing the costs of bioanalysis as well as drug discovery and development; (3) some of the substrates used in microfluidic devices have high O_2 permeability which has an important impact on cell proliferation and (4) this technology allows the integration of numerous features namely cell culture and sampling, control of fluids, capturing of cells, cell lysis as well as mixing and detection all on one single device.[76,77] The various microfluidic platforms that have been previously used in 3D cell cultures include glass/silicon-based, polymer-based together with paper-based platforms, which

Table 1 Summary of PDT studies in 3D *in vitro* cancer models

Photosensitiser	Description of 3D cancer model	Cancer cell line	Ref.
Methylene blue	Spheres on (poly 2-hydroxyethyl methacrylate) (polyHEMA) coated microwells in a microfluidic device	Human breast carcinoma (T47D)	91
Benzoporphyrin Derivative (BPD)	Micronodules on Matrigel matrix	Human ovarian carcinoma (OVCAR5)	92
5-Ethylamino-9-diethylaminobenzo[*a*] phenothiazinium chloride (EtNBS)	Nodules on growth factor reduced (GFR) Matrigel matrix	Human ovarian carcinoma (OVCAR5)	93
BPD in DMSO	Micronodules on Matrigel matrix	Human ovarian carcinoma (OVCAR5)	94
BPD	Micronodules on Matrigel matrix	Human ovarian carcinoma (OVCAR5)	95
5-Aminolevulinic acid (5-ALA)	Nodules on Matrigel matrix	Human epidermal carcinoma (A431)	35
BPD, mono-*N*-aspartyl derivative of chlorin e6 (MACE)	Mammary architecture and micro-environment engineering (MAME) of breast cancer Spheroids formed on glass cover slips coated with reconstituted basement membrane	Human breast carcinoma (SUM149, MDA-MB-231, Hs578T)	96
Tetraphenyl disulfonated porphyrin ($TPPS_{2a}$), disulfonated tetraphenyl chlorin ($TPCS_{2a}$)	Single cells seeded in hydrogel (collagen) scaffold	Human prostate adenocarcinoma (PC3)	97
Tetraphenyl disulfonated porphyrin ($TPPS_{2a}$), disulfonated tetraphenyl chlorin ($TPCS_{2a}$)	Single cells seeded in hydrogel (collagen) scaffold	Human head and neck squamous cell carcinoma (PCI30)	98
*m*THPC	Single cells seeded in hydrogel (collagen) scaffold	Human breast carcinoma (MCF-7)	99
BPD	Nodules on Matrigel	Human ovarian carcinoma (OVCAR5)	100
Hypericin	Spheroid on agarose coating	Human bladder carcinoma (RT-112)	101
Ruthenium(II) polypyridyl complexes (Ru1–Ru3)	Spheroid on agarose coating	Human cervical carcinoma (HeLa)	102
Ruthenium(II) polypyridyl complexes (RuL1–RuL4)	Spheroid on agarose coating	Human cervical carcinoma (HeLa)	103
Fluorinated ruthenium(II) complexes (Ru1–Ru5)	Spheroid using liquid overlay method	Human cervical carcinoma (HeLa)	104

Open Access Article. Published on 08 2018. Downloaded on 09-08-2025 20:27:54.
This article is licensed under a Creative Commons Attribution 3.0 Unported Licence.

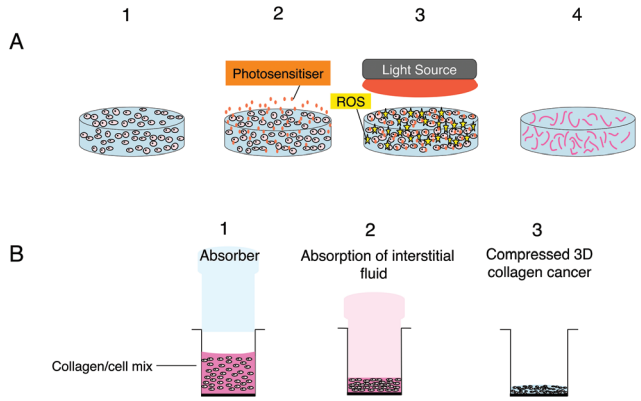

Fig. 1 (A) PDT using nanoparticles in 3D hydrogel model consisting of cancer cells surrounded by a matrix (*e.g.* type 1 rat tail collagen) illustrated with sequential procedures; step 1: seeding of cancer cells in the hydrogel scaffold; step 2, addition of a photosensitiser for cell uptake followed by washing; step 3: the irradiation of the 3D model with light and generation of ROS. Step 4: the dead cancer cells in the hydrogel scaffold. (B) Construction of compressed 3D collagen cancer models with higher collagen density for therapeutic studies illustrated sequentially. Step 1, the formation of collagen/cell mix prior to undergoing the plastic compression stage using an insertable absorber to extract fluid from the hydrogel; step 2 shows the gradual absorption of the interstitial fluid from the collagen/cell mix by the absorber and the slow compression of the model; step 3 demonstrates the thinner (typically 200 μm depth) compressed 3D collagen cancer model following the absorption of the fluid from the model resulting in a ten-fold higher collagen density.

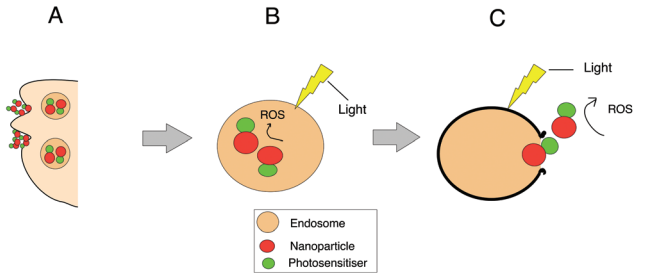

Fig. 2 Endocytic uptake and reactive oxygen species (ROS) generation for nanoparticles conjugated with the photosensitiser. (A) Uptake of photosensitiser conjugated nanoparticles by the cell *via* endocytosis and their localisation within endosomes and subsequently lysosomes. (B) Light-induced generation of ROS within the endosome containing the conjugates where they interact with the membrane and other components inside the organelle. Some ROS may also migrate through the membrane of the endososome where they can oxidise other substrates in the cell. (C) Photo-induced rupture of the endo/lysosomal membrane after prolonged irradiation *via* interaction of ROS with the membrane, leading to the escape of the nanoparticle into the cytosol and production of ROS at other intracellular sites.

have been named depending on the substrates used in the fabrication of the micro-device.[75] Such technology has also been used for photo-oxidation reaction studies related to PDT.[78]

Scaffolds

3D scaffolds consisting of a nano-fibrous matrix create an environment, which supports the proliferation, growth as well as migration of cancer cells allowing such aspects to be investigated.[79] Scaffolds present several advantages over spheroids in particular the capability of mimicking tumour heterogeneity as well as the control of the 3D dimensions. Furthermore the extent of migration, proliferation and aggregation of the cells can be controlled by the surface properties as well as the composition, configuration and the porosity of the scaffolds.[79,80] These properties also make such models good candidates for nanocarrier delivery studies as shown by the work of Lopez *et al.* (2016)[81] which focused on the diffusion properties of liposomes and micelles in a 3D collagen scaffold model.[81] Scaffolds can be subdivided into natural or synthetic scaffolds based on the materials incorporated therein.[82]

Natural scaffolds are largely hydrogels containing mostly water[83] and natural components such as collagen type 1 (Fig. 2), matrigel, agarose, elastin, laminin and hyaluronic acid.[71,84] Although mechanically weak due to the high volume of excess fluid with them, hydrogel models permit the movement and proliferation of cells within a biological environment.[79] However their low density does not reflect the dense environment surrounding tumour cells *in vivo*.[79] This problem can be resolved in part by the remodelling of the hydrogel to assist cell–matrix interaction studies and a rise in matrix density due to contraction.[85] The development of the plastic compression technology has resulted in the production of improved biomimetic scaffolds with increased cell and collagen density through the removal of interstitial fluid from the hydrogel model.[86] The collagen stiffness in these scaffolds not only influences rate of cell growth as well as morphologies,[87] but owing to the higher collagen density and reduced oxygen diffusion also enables the hypoxic core that is normally observed *in vivo* to be imitated *in vitro*.[79] Fig. 2 exemplifies the stages involved in the formation of the compressed 3D model. Recent studies with compressed collagen hydrogels have utilised 'tumouroid' models consisting of a cancer mass surrounded by a multi-cellular stroma to study the uptake of nanoparticles in addition to their use in enhancing drug delivery.[81,88]

Synthetic scaffolds can also be developed from polymers *e.g.* polyactide (PLA), polyglycolide (PGA) and co-polymers (PLGA).[82] These polymers are biodegradable and can be manipulated to create a variety of structures such as mesh, fibers and sponge.[89] Synthetic scaffolds have a stronger mechanical structure than natural scaffolds and can specifically replicate biomolecular structures seen *in vivo*.[90] Cell adhesions are unfortunately weaker on these polymers and therefore surface modifications are required to overcome this problem.[79]

PDT applications in 3D cancer models

There is growing interest in the use of 3D models to better replicate the cellular response to PDT and overcome some of

 This journal is © The Royal Society of Chemistry 2018

Open Access Article. Published on 08 2018. Downloaded on 09-08-2025 20:27:54.
This article is licensed under a Creative Commons Attribution 3.0 Unported Licence.

the limitations of conventional monolayer culture. A further motivation is that the use of 3D models and their rapid screening capability could reduce the need expensive *in vivo* experimentation. 3D cancer models, particularly using spheroid cultures have contributed to photodynamic research by allowing the uptake and the therapeutic efficacy of various photosensitisers to be examined.[66] More recently, microfluidic technology has been applied to PDT.[91] Since PDT efficacy is dependent on an adequate oxygen supply, investigation of the PDT response at lower oxygen levels found in solid tumours is particularly relevant. Moreover the PDT process consumes molecular oxygen as molecular substrates become oxidised, thus diffusion and consumption of oxygen within a tissue construct can mimic the *in vivo* dynamics.[13] Regarding visible light penetration within the 3D models, since the constructs are relatively thin (typically <1 mm) partly in order to permit oxygen replenishment, attenuation of the light for PDT activation is negligible.

Table 1 presents a summary of experimental data obtained using 3D *in vitro* cancer models and a range of photosensitisers administered in solution form. The description of the 3D cancer model (*e.g.* spheroid, micronodule *etc*.) uses the terminology given in the quoted reference articles.

In several studies differences were noted between cellular responses to PDT in 2D and 3D culture models. For example, Chen *et al.* (2015)[91] used the microfluidic platform to create a breast cancer sphere culture environment on a chip using T47D cells. The formation of such spheres was a consequence of aggregation of cells in each individual microwell. The 3D cultures were incubated with photosensitiser methylene blue at a concentration of 10 μM for 1 hour before undergoing illumination for different periods. The results showed that after 10 minutes under an exposure dose of 7.3 J cm^{-2} approximately 50% cell kill was attained in the 2D cell monolayer while in the 3D spheres a majority of the cells were viable. Even after the longest illumination period of 1 hour and highest light dose (44 J cm^{-2}) a portion of the T47D cells within the centre of the spheres were still viable. The larger spheres demonstrated more resistance towards PDT under the same therapeutic conditions than small spheres indicating the effect of sphere size on PDT efficacy. The penetration of the photosensitiser and the lower oxygen levels prevalent at the interior of the spheroid are both factors limiting the PDT efficacy in larger spheroids.

A different study carried out by Rizvi *et al.* (2013)[95] focused on using BPD-PDT in 3D tumour models of ovarian cancer, which consisted of micronodules of OVCAR5 human cancer cultures developed on growth factor reduced (GFR) Matrigel. The models were incubated with 0.25 μM, 1 μM and 10 μM BPD for 90 minutes prior to undergoing irradiation using a 690 nm fibre-coupled diode laser. Significant reduction in cell viability occurred in nodules that were treated with 0.25 μM BPD-PDT mainly after 72 hours and 96 hours post treatment compared to nodules treated with 1 μM and 10 μM BPD-PDT. However nodules that underwent therapy with a higher concentration of 10 μM BPD-PDT exhibited the poorest response. This result may have been due to aggregation of the photosensitiser, which can impair its photosensitising efficacy, as well as other microenvironmental factors.

In another recent study conducted by Evans *et al.* (2011),[93] the ovarian cancer cell line OVCAR5 was again used to develop spheroids on GFR containing Matrigel to investigate the effect of PDT using photosensitiser 5-ethylamino-9-diethylaminobenzo[*a*] phenothiazinium chloride (EtNBS) on hypoxic cell populations within 3D tumour models of ovarian cancer. The spheroids were incubated with 500 nM EtNBS for 4.5 hours to allow the photosensitiser to concentrate into the core cell populations within the spheroid. At a light dose of 5 J cm^{-2}, EtNBS managed to selectively destroy the spheroid core cells. This shows EtNBS is able to both concentrate into and destroy the hypoxic cell populations that are normally difficult to treat. At higher doses of light EtNBS-PDT was capable of causing cell killing across the entire model indicating that such therapy is effective against both hypoxic and normoxic regions of a tumour. Interestingly the uptake and cytotoxicity of EtNBS was found to increase with expansion of spheroid size mainly owing to the rise in the hypoxic populations found in the larger spheroids. These results demonstrate the utility of 3D models for testing PDT efficacy under lower oxygen partial pressures that apply *in vivo* in contrast to conventional 2D model testing, and together with Chen *et al.*,[91] exemplify the advantages of using the 3D architecture of these biomimetic models to obtain a clearer understanding of processes relevant to *in vivo* experimentation.

The use of nanoparticles in PDT and their applications in 3D cancer models

Localised treatment with minimal side effects as well as the lack of mutagenicity and mild allergenicity are in principle key advantages of using photosensitisers. However it is recognized that there are several limitations such as the lack of sufficient tumour selectivity and poor bioavailability which has led to the development of nanoparticle delivery systems in PDT.[61,105] For example, the bioavailability of otherwise water insoluble photosensitisers may be improved using a water soluble 'nanocarrier' thereby enabling intravenous administration. Nanocarriers can be "actively" targeted to the diseased site using surface-conjugated ligands that bind to overexpressed receptors or antigens on the target tissue.[105–110] Improved tumour targeting is also possible *via* the enhanced permeability and retention (EPR) properties of nanoparticles, a process that is termed "passive" targeting selectivity. In this case, the targeting of photosensitisers can be commonly achieved through encapsulation or conjugation to nanocarriers such as liposomes or polymeric particles. Alternatively, the photosensitisers can be covalently bound to the surface of the nanoparticle (*e.g.* silica) or within the matrix *via* either a stable bond or a biodegradable linkage so that the photosensitiser can migrate elsewhere within the cell following uptake of the nanoparticle. If the matrix of the nanoparticle is bio-

Open Access Article. Published on 08 2018. Downloaded on 09-08-2025 20:27:54.
This article is licensed under a Creative Commons Attribution 3.0 Unported Licence.

degradable, the photosensitiser release occurs either within the cell or during circulation. Owing to their size, nanoparticles are generally taken up *via* endocytosis as shown in Fig. 2. If the photosensitiser remains entrapped with the nanoparticle during cell uptake, ROS are then photogenerated within the endo/lysosomes, as depicted in Fig. 2. With a sufficient light dose the membrane will be ruptured enabling the nanoparticles to migrate from the endo/lysosomes. Nanoparticles can also act as photocatalytic agents or photosensitisers themselves, in effect as 'nanophotosenstisers' to generate reactive oxygen species.[111–113] Examples include metallic or semiconducting nanoparticles and organic fullerenes.[111,112] In combination with a dye, Förster resonance energy transfer (FRET) can also occur with light-activated nanoparticle.[112,114,115] A wide range of nanocarriers have been tested, from inorganic to organic compositions. Example of inorganic nanocarriers include single-wall carbon nanotubes (SWCNTs),[116] upconversion nanoparticles ($NaYF_4$:Yb^{3+},Er^{3+})[117] and self-lighting nanoparticles ($NaYF_4$:Yb^{3+},BaFBr:Eu^{2+},Mn^{2+}, LaF_3:Tb^{3+}).[116] Nanoparticles can also be sub-classified into either biodegradable (alginate, chitosan, cyclodextrin, albumin PLA, PLGA)[118,119] or non-biodegradable (polyacrylamide, silica, gold (Au), iron oxide) nanoparticles.

In 3D cultures, both oxygen and nanoparticle delivery are controlled by diffusion to the cells through the matrix following administration to the surface of the construct. In principle therefore 3D models are well suited to studying the efficacy of nanoparticles for PDT. Incorporation of a vascular network is still in its infancy and remains a longer term goal.[120] Numerous studies have investigated the properties of nanoparticles to improve the therapeutic effects obtained from PDT treatment of various cell types in 3D models. Table 2 provides examples of nanoparticles used in PDT studies that have been carried out in 3D cancer models. A key benefit of employing 3D models for PDT studies involving nanoparticles is their ability to incorporate the cell penetration problems experienced by nanoparticles in contrast with 2D monolayer cultures.[25]

The various types of photosensitisers in nanoparticle form that have been studied in 3D cancer models are listed in Table 2. The nanoparticles used range from inorganic (gold), micelles, polymeric carriers, liposomes and two types of carbon-based particles. Studies shown in some cases included comparisons between 2D and 3D models. For example, Yang *et al.* (2015)[121] employed a 3D breast cancer tissue model comprised of human breast cancer cells (MCF-7) as well as primary adipose-derived stromal cells (ASCs) using a microfluidic device (Fig. 3) to study the synergistic enhancement of PDT using a combination of 5-ALA and AuNPs. The distribution profiles of the agents and influence of light penetration on PDT according to depth of the cancer tissue were also investigated. The breast cancer tissues underwent incubation with 1 mM 5-ALA dissolved in a serum free medium either with or without AuNPs for 4 hours. For comparison the same PDT treatment conditions were also applied on MCF-7 cells in 2D. When 5-ALA was administered alone, PDT gave approximately 50% cell kill in 2D monolayer culture and 17% cell kill in 3D culture compared to higher cell kill of 70% and 50% achieved respectively in the presence of AuNPs. By extending the illumination period most of the cells in the 2D monolayer were destroyed with or without the AuNPs, whereas in the 3D culture with 5-ALA alone was less effective with 50% kill compared to 90% kill with the AuNPS present. Generally much higher cell destruction was observed in the 2D culture compared to the 3D model throughout all illumination periods. Such evidence for synergistic cell kill with 5-ALA/AuNP com-

Table 2 Summary of PDT studies in 3D *in vitro* cancer models involving nanoformulated photosensitisers

Photosensitiser	Nanoparticle	Description of 3D cancer model	Cancer cell line	Ref.
5-Aminolaevulinic acid (5-ALA) induced PPIX	Gold nanoparticle (AuNPs)	Nodules on microfluidic device	Human breast carcinoma (MCF-7)	121
Pheophorbide A (Pheo)	Micelles poly (ethyleneoxide-*b*-3-caprolactone)	Spheroid on ultra-low attachment well plates	Human colorectal carcinoma (HCT-116), human squamous cell carcinoma (FaDu)	68
m-Tetrahydroxyphenylchlorin (*m*THPC)	Lipidots	Spheroid using hanging drop method	Human tongue squamous cell carcinoma (CAL-33)	69
EtNBS	Poly(lactic-*co*-glycolic acid) (PLGA)	Spheroid on Matrigel	Human ovarian carcinoma (OvCAR)	122
cis–Bis(2, 2′-bipyridine) dichlororuthenium(II) hydrate	SWCNTs	Spheroid using liquid overlay method	Human cervical carcinoma (HeLa)	123
Chlorin e_6 (Ce6)	Reduced graphene oxide (rGO)	Spheroid	Human brain carcinoma (U87)	124
m-THPC	Liposome (Foslip™ and Fospeg™)	Spheroid using liquid overlay method	Human cervical carcinoma (HeLa)	125
Zinc phthalocyanine (ZnPc)	Liposome	Spheroid on agarose coating	Human cervix adenocarcinoma (HeLa cells) and mouse Mus musculus colon carcinoma (CT26)	126
Photofrin	Liposome	Spheroid using spinner flasks on a stir-plate	Human bladder carcinoma (MGHU3)	127
Indocyanine green	PLGA/lipid	Spheroid on agarose coating	Mouse breast carcinoma (4T1)	128

 This journal is © The Royal Society of Chemistry 2018

Open Access Article. Published on 08 2018. Downloaded on 09-08-2025 20:27:54.
This article is licensed under a Creative Commons Attribution 3.0 Unported Licence.

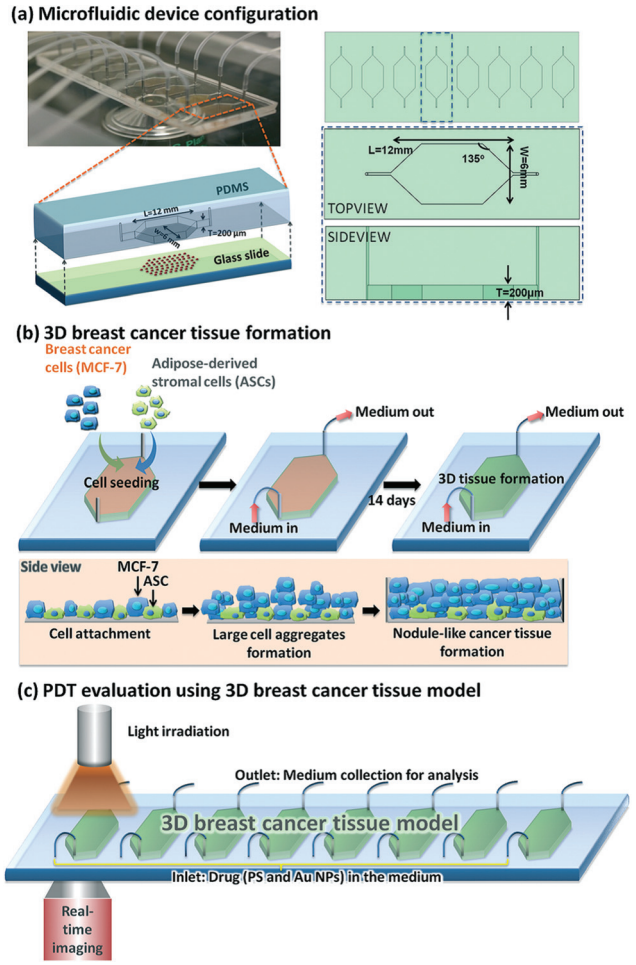

Fig. 3 Microfluidic device design and PDT application using Au NPs. (a) Left top: Optically transparent microfluidic device on the stage of a time-lapse microscope within a climate control incubator. Left bottom: Configuration of our microfluidic device for 3D breast cancer tissue formation in which polydimethylsiloxane serves as the housing material and glass slide serves as the substrate. Right: Schematic layout of eight chambers on a 3″ × 1″ glass slide with defined parameters for the chamber design. (b) Conceptual illustration of the development of MCF-7 and ASCs cells into 3D breast cancer tissue within the microfluidic chambers. (c) Experimental setup for PDT evaluation using the microfluidic breast cancer tissue model, in which the photosensitiser (PS) and Au NPs are introduced into the system together with a cell culture medium *via* the inlet, and light irradiation is realised by exposing the transparent device to the light source from the top. Reprinted with permission from ref. 121 (Fig. 1, Y. Yang, X. Yang, J. Zou, C. Jia, Y. Hu, H. Du, H. Wang, *Lab Chip*, 2015, **15**, 735–44).

bined PDT has also been confirmed by Benito *et al.* (2013).[129] Yang *et al.* (2015)[121] also observed a more homogenous response where the dead cells were found to be distributed across the full thickness of the cancer tissue in the 3D model post-treatment with 5-ALA and AuNPs combined, whereas with 5-ALA-only PDT, a majority of the dead cells were identified within the superficial parts of the cancer tissue.

Till *et al.* (2016)[68] on the other hand used 3D spheroid models developed from human colorectal carcinoma cell line (HCT-116) and human squamous cell carcinoma cell line (FaDu) on ultra-low attachment plates for investigating PDT efficacy. This study compared PDT using a pheophorbide photosensitiser (Pheo) in free solution form to the use of encapsulated photosensitiser in crosslinked polymeric micellar self-assemblies *versus* uncrosslinked micellar counterparts. In this experiment the spheroids were incubated with photosensitiser in free or encapsulated form for 30 minutes before undergoing irradiation for 8 minutes. The spheroids were exposed to two further cycles of 8-minute irradiation every 24 hours for two days after the first cycle of irradiation. Using the photosensitiser in free form led to low PDT efficiency as a result of its aggregation in water, with a lower response in FaDu spheroids and in HCT-116 spheroids only a 35% decrease in spheroid size was achieved after the third cycle of irradiation. PDT treatment of the spheroids using encapsulated pheophorbide was more effective than free photosensitiser, and the crosslinked systems were more effective compared to the uncrosslinked nanovectors. Different results were obtained in 2D at low concentration where the uncrosslinked micelles were found to elicit better cell kill. The authors noted that *in vivo* studies of crosslinked *vs.* uncrosslinked micelles bearing chemotherapeutics have shown that the crosslinked micelles are more effective, which supports their contention that the 3D model better simulated the *in vivo* response.

In an attempt to minimise the dark toxicity of EtNBS and examine its potential as a PDT photosensitser, Hung *et al.* (2016)[122] encapsulated EtNBS in PLGA NPs and tested this formulation in OVCAR5 monolayer and spheroid models. In monolayer culture, EtNBS loaded nanoparticles showed reduced dark toxicity compared to cells treated with free EtNBS. Uptake studies in the spheroids demonstrated the diffusion of PLGA-EtNBS throughout the spheroids in the same way as free EtNBS and the release of the photosensitiser from PLGA upon illumination with laser light of 635 nm wavelength. PDT using PLGA-EtNBS delivery was still effective even in hypoxic cellular microenvironments present in the spheroid models, with comparable efficacy to free EtNBS. Zhang *et al.* (2015)[123] studied Ru(II) complex loaded SWCNTs (Ru@SWCNTs) as an approach for inducing photothermal and two-photon photodynamic therapy (PTT/TPPDT) effects in HeLa cervical cancer spheroid models. The closely packed cells in spheroids make this type of model particularly suitable for demonstrating the optical sectioning capabilities of multiphoton PDT. After incubation with Ru@SWCNTs (50 µg ml^{-1}) excitation with 808 nm laser irradiation led to a reduction in the mean diameter of the spheroids and significant loss in cell viability. Liu *et al.* (2017)[124] investigated loading chlorin e_6 onto rGO to study PTT and PDT efficacy in 3D U87 cell spheroid models. Although both therapies proved effective on 2D cultures of U87 cells, only PTT demonstrated a considerable treatment efficacy in the spheroid models.

Owing to their ability to encapsulate either lipophilic and hydrophilic compounds and other advantages, liposomes have been used in several PDT studies on 3D cancer spheroid models.[125–127] For example Gaio *et al.* (2016)[125] investigated the photo-induced damage of two liposomal formulations of

Open Access Article. Published on 08 2018. Downloaded on 09-08-2025 20:27:54.
This article is licensed under a Creative Commons Attribution 3.0 Unported Licence.

m-THPC, Foslip® and Fospeg® compared to Foscan® in 3D HeLa spheroid models. Confocal fluorescence microscopy showed that *m*-THPC penetration was limited and mainly confined to the external cell layers of spheroids with a slightly higher accumulation of Foslip® and Fospeg® with respect to Foscan®. A significant reduction in cell viability of the spheroids was observed in models incubated in the dark with Foscan (8 μM) while the spheroids treated with the liposomal formulations did not elicit dark toxicity. After PDT the cell viabilities of the spheroids were greatly reduced with all three different formulations with Foslip® showing the most reduction in viability at each time point.

As mentioned in the Introduction,[16,25] a key advantage of 3D models is their utility for studying drug and nanoparticle penetration. López-Dávila *et al.*[81] used confocal fluorescence microscopy of a Nile Red dye and DNA photosensitiser in free form (DMSO solution) or incorporated in micelles and liposomes to study the depth of dye penetration over a 24 hours period into compressed collagen hydrogels containing a colorectal cancer mass. The rate of diffusion of the free dye determined using fluorescence imaging was significantly higher than observed with either of the nanoparticles, which had similar distributions. An advantage of using a compressed hydrogel (Fig. 1b) for penetration and diffusion studies is that the collagen density (weight/volume) is much higher and closer to physiological levels, whereas for a standard uncompressed collagen hydrogel the density is <0.5%. Most of the nanoparticle PDT studies mentioned in Table 2 have been carried out on spheroid models and useful new information has been obtained with these models. However replication of drug and medium perfusion through tissue in 3D models remains challenging although microfluidic models appear to provide a promising approach, although further studies are needed.

Conclusions

The development of new photosensitisers that can be activated at longer wavelengths and their incorporation in nanoparticles for PDT has led to a surge of interest in this field over recent years. 3D cancer models provide the opportunity to carry out more physiologically realistic studies of minimally invasive methods such as photodynamic therapy and help bridge the gap between *in vitro* and *in vivo* studies. As exemplified by the studies covered in this review, exploiting the biomimetic properties of 3D models can counter overestimation of photosensitising efficacy observed with 2D monolayer model studies by taking account of the limited drug/nanoparticle penetration through the extracellular matrix.

PDT is generally used for treatment of solid tumours where hypoxia and treatment-induced oxygen consumption may limit treatment efficacy. The ability of 3D models to simulate normoxic *vs.* hypoxic conditions and light dosimetry planning are all factors that will encourage further use of 3D models of solid cancer for PDT studies. In this review we have focused on biomimetic constructs, which are much cheaper to prepare than carrying out rodent tumour model studies. However we note that another approach, which is also relatively inexpensive, based on zebrafish tumour models has been tested using nanoparticle-mediated PDT recently that may prove useful in future.[130]

Future prospects

With rapid advances being made in developing more sophisticated 3D tissue culture systems, their application will be increasingly exploited for PDT and related studies relying on photoactivation. The development of perfusable vascularised constructs will be particularly useful for PDT studies since vascular damage induced by PDT plays a key role for many photosensitisers. There is increasing interest in the combination of PDT as part of a combination therapy in particular its use with other agents such as chemotherapeutics,[106] where 3D models may prove useful since the cellular response to the chemotherapeutics may also be better simulated in the 3D model. In this approach the photosensitiser and agent may be co-delivered using one nanocarrier and comparison of these methods *versus* separate administration should be studied using 3D models. In a related development, PDT may also be used to enhance drug delivery using a technique known as photochemical internalisation (PCI), which relies on the photosensitiser being localised in endolysosomal membranes. PCI can improve the intracellular delivery of a macromolecular drug or nanocarrier entrapped within endolysosomes to the cytosol potentially leading to a higher therapeutic effect than using PDT alone.[131,132] From the mechanistic point of view, the interaction between tumour and stromal components such as tumour-associated fibroblasts and their contribution to the tumour cell response may also be elucidated better using 3D model technology. This approach will also be useful for non-PDT photoactivatable agents such as a ruthenium-caged photosensitiser for cathepsin K inhibition, where the spatiotemporal control over activation that can be exerted using a 3D model has been demonstrated recently.[133] Two photon activation of photosensitisers using ultrafast laser excitation is another area that will benefit from the use of 3D models since it will be easier to demonstrate the optical sectioning selectivity conferred using two photon *versus* one photon excitation.[134]

Conflicts of interest

There are no conflicts of interest to declare.

Acknowledgements

We acknowledge support for EY from Innovate UK and the Medical Research Council under the Biomedical Catalyst scheme (grant number 101875) and funding from the NIHR

 This journal is © The Royal Society of Chemistry 2018

i4i Scheme (grant number II-LA-0813-20002). We also thank Amir Afrashtehpour for his help in the preparation of the manuscript.

References

1 D. E. Dolmans, D. Fukumura and R. K. Jain, *Nat. Rev. Cancer*, 2003, **3**, 380–387.
2 A. R. Azzouzi, S. Vincendeau, E. Barret, A. Cicco, F. Kleinclauss, H. G. van der Poel, C. G. Stief, J. Rassweiler, G. Salomon, E. Solsona, A. Alcaraz, T. T. Tammela, D. J. Rosario, F. Gomez-Veiga, G. Ahlgren, F. Benzaghou, B. Gaillac, B. Amzal, F. M. Debruyne, G. Fromont, C. Gratzke and M. Emberton, *Lancet Oncol.*, 2017, **18**, 181–191.
3 S. Mallidi, S. Anbil, A. L. Bulin, G. Obaid, M. Ichikawa and T. Hasan, *Theranostics*, 2016, **6**, 2458–2487.
4 H. Abrahamse and M. R. Hamblin, *Biochem. J.*, 2016, **473**, 347–364.
5 P. Agostinis, K. Berg, K. A. Cengel, T. H. Foster, A. W. Girotti, S. O. Gollnick, S. M. Hahn, M. R. Hamblin, A. Juzeniene, D. Kessel, M. Korbelik, J. Moan, P. Mroz, D. Nowis, J. Piette, B. C. Wilson and J. Golab, *CA-Cancer J. Clin.*, 2011, **61**, 250–281.
6 C. Hopper, *Lancet Oncol.*, 2000, **1**, 212–219.
7 H. Nyst, I. Tan, F. Stewart and A. Balm, *Photodiagn. Photodyn. Ther.*, 2009, **6**, 3–11.
8 S. B. Brown, E. A. Brown and I. Walker, *Lancet Oncol.*, 2004, **5**, 497–508.
9 R. Misra, S. Acharya and S. K. Sahoo, *Drug Discovery Today*, 2010, **15**, 842–850.
10 A. Nyga, M. Loizidou, M. Emberton and U. Cheema, *Acta Biomater.*, 2013, **9**, 7917–7926.
11 C. Hsieh, Y. Chen, S. Huang, H. Wang and M. Wu, *BioMed Res. Int.*, 2015, **2015**, 1–10.
12 H. L. Ma, Q. Jiang, S. Han, Y. Wu, J. Cui Tomshine, D. Wang, Y. Gan, G. Zou and X. J. Liang, *Mol. Imaging*, 2012, **11**, 487–498.
13 M. Alemany-Ribes, M. Garcia-Diaz, M. Busom, S. Nonell and C. E. Semino, *Tissue Eng., Part A*, 2013, **19**, 1665–1674.
14 M. Zanoni, F. Piccinini, C. Arienti, A. Zamagni, S. Santi, R. Polico, A. Bevilacqua and A. Tesei, *Sci. Rep.*, 2016, **6**, 19103.
15 M. Zhang, P. Boughton, B. Rose, C. Lee and A. Hong, *Int. J. Biomater.*, 2013, **2013**, 1–9.
16 X. Xu, C. R. Sabanayagam, D. A. Harrington, M. C. Farach-Carson and X. A. Jia, *Biomaterials*, 2014, **35**, 3319–3330.
17 B. Keith and M. C. Simon, *Cell*, 2007, **129**, 465–472.
18 R. Edmondson, J. Broglie, A. Adcock and L. Yang, *Assay Drug Dev. Technol.*, 2014, **12**, 207–218.
19 K. M. Yamada and E. Cukierman, *Cell*, 2007, **130**, 601–610.
20 D. Antoni, H. Burckel, E. Josset and G. Noel, *Int. J. Mol. Sci.*, 2015, **16**, 5517–5527.
21 V. van Duinen, S. J. Trietsch, J. Joore, P. Vulto and T. Hankemeier, *Curr. Opin. Biotechnol.*, 2015, **35**, 118–126.
22 D. Huh, G. A. Hamilton and D. E. Ingber, *Trends Cell Biol.*, 2011, **21**, 745–754.
23 C. S. Shin, B. Kwak, B. Han and K. Park, *Mol. Pharmaceutics.*, 2013, **10**, 2167–2175.
24 J. P. Celli, I. Rizvi, A. R. Blanden, I. Massodi, M. D. Glidden and B. W. Pogue, *Sci. Rep.*, 2014, **4**, 3751.
25 J. Zhao, H. Lu, B. Sandy Wong, M. Lu, P. Xiaob and M. H. Stenze, *Polym. Chem.*, 2017, **8**, 3317–3326.
26 P. Acedo, J. C. Stockert, M. Canete and A. Villanueva, *Cell Death Dis.*, 2014, **5**, 1122.
27 A. E. O'Connor, W. M. Gallagher and A. T. Byrne, *Photochem. Photobiol.*, 2009, **85**, 1053–1074.
28 T. A. Slastnikova, A. A. Rosenkranz, T. N. Lupanova, P. V. Gulak, N. V. Gnuchev and A. S. Sobolev, *Dokl. Biochem. Biophys.*, 2012, **446**, 235–237.
29 D. Kessel, *Photochem. Photobiol. Sci.*, 2015, **14**, 1397–1402.
30 D. Kessel and N. L. Oleinick, *Methods Mol. Biol.*, 2010, **635**, 35–46.
31 S. Marchal, A. Fadloun, E. Maugain, M. D'Hallewin, F. Guillemin and L. Bezdetnaya, *Biochem. Pharmacol.*, 2005, **69**, 1167–1176.
32 D. Kessel, *Autophagy*, 2015, **11**, 1941–1943.
33 I. O. Bacellar, T. M. Tsubone, C. Pavani and M. S. Baptista, *Int. J. Mol. Sci.*, 2015, **16**, 20523–20559.
34 A. Juarranz, P. Jaen, F. Sanz-Rodriguez, J. Cuevas and S. Gonzalez, *Clin. Transl. Oncol.*, 2008, **10**, 148–154.
35 J. Hempstead, D. P. Jones, A. Ziouche, G. M. Cramer, L. Rizvi and S. Arnason, *Sci. Rep.*, 2015, **5**, 10093.
36 T. Kushibiki, T. Tajiri, Y. Tomioka and K. Awazu, *Int. J. Clin. Exp. Med.*, 2010, **3**, 110–114.
37 H. Ding, H. Yu, Y. Dong, R. Tian, G. Huang and D. A. Boothman, *J. Controlled Release*, 2011, **156**, 276–280.
38 R. Yin, T. Agrawal, U. Khan, G. K. Gupta, V. Rai, Y. Y. Huang and M. R. Hamblin, *Nanomedicine*, 2015, **10**, 2379–2404.
39 M. Triesscheijn, P. Baas, J. H. Schellens and F. A. Stewart, *Oncologist*, 2006, **11**, 1034–1044.
40 F. Selvestrel, F. Moret, D. Segat, J. H. Woodhams, G. Fracasso, I. M. Rio Echevarria, L. Bau, F. Rastrelli, C. Compagnin, E. Reddi, C. Fedeli, E. Papini, R. Tavano, A. Mackenzie, M. Bovis, E. Yaghini, A. J. MacRobert, S. Zanini, A. Boscaini, M. Colombatti and F. Mancin, *Nanoscale*, 2013, **5**, 6106–6116.
41 R. M. Valentine, K. Wood, C. T. Brown, S. H. Ibbotson and H. Moseley, *Phys. Med. Biol.*, 2012, **57**, 6327–6345.
42 S. Mallidi, Z. Mai, I. Rizvi, J. Hempstead, S. Arnason, J. Celli and T. Hasan, *J. Biomed. Opt.*, 2015, **20**, 048003.
43 S. Parker, *Br. Dent. J.*, 2013, **215**, 167–171.
44 R. Toftegaard, J. Arnbjerg, K. Daasbjerg, P. R. Ogilby, A. Dmitriev, D. S. Sutherland and L. Poulsen, *Angew. Chem., Int. Ed.*, 2008, **47**, 6025–6027.
45 Y. Y. Huang, S. K. Sharma, R. Yin, T. Agrawal, L. Y. Chiang and M. R. Hamblin, *J. Biomed. Nanotechnol.*, 2014, **10**, 1918–1936.

Open Access Article. Published on 08 2018. Downloaded on 09-08-2025 20:27:54.
This article is licensed under a Creative Commons Attribution 3.0 Unported Licence.

Open Access Article. Published on 08 2018. Downloaded on 09-08-2025 20:27:54.
This article is licensed under a Creative Commons Attribution 3.0 Unported Licence.

46 A. Oseroff, L. Blumenson, B. Wilson, T. Mang, D. Bellnier, J. Parsons, N. Frawley, M. Cooper, N. Zeitouni and T. A. Dougherty, *Lasers Surg. Med.*, 2006, **38**, 417–426.
47 J. Usuda, H. Kato, T. Okunaka, K. Furukawa, H. Tsutsui and K. Yamada, *J. Thorac. Oncol.*, 2006, **1**, 489–493.
48 M. Tanaka, H. Kataoka, M. Mabuchi, S. Sakuma, S. Takahashi and R. Tujii, *Anticancer Res.*, 2011, **31**, 763–769.
49 M. J. Bovis, J. H. Woodhams, M. Loizidou, D. Schegglmann, S. G. Bown and A. J. MacRobert, *J. Controlled Release*, 2012, **157**, 196–205.
50 B. J. Qumseya, W. David and H. C. Wolfsen, *Clin. Endosc.*, 2013, **46**, 30–37.
51 C. Hopper, A. Kubler, H. Lewis, I. B. Tan and G. Putnam, *Int. J. Cancer.*, 2004, **111**, 138–146.
52 D. Meier, C. Campanile, S. M. Botter, W. Born and B. Fuchs, *J. Visualized Exp.*, 2014, **18**, DOI: 10.3791/51213.
53 W. Jerjes, Z. Hamdoon and C. Hopper, *Head Neck Oncol.*, 2012, **4**, 16.
54 L. B. Josefsen and R. W. Boyle, *Br. J. Pharmacol.*, 2008, **154**, 1–3.
55 Z. Huang, *Technol. Cancer Res. Treat.*, 2005, **4**, 283–293.
56 I. Yoon, J. Z. Li and Y. K. Shim, *Clin. Endosc.*, 2013, **46**, 7–23.
57 A. B. Ormond and H. S. Freeman, *Materials*, 2013, **6**, 817–840.
58 A. K. Bhatta, U. Keyal and X. L. Wang, *Photodiagn. Photodyn. Ther.*, 2016, **15**, 228–235.
59 C. Poriel, D. Kessel and M. G. Vicente, *Photochem. Photobiol.*, 2005, **81**, 149–153.
60 R. R. Allison, G. H. Downie, R. Cuenca, X. H. Hu, C. J. Childs and C. H. Sibata, *Photodiagn. Photodyn. Ther.*, 2004, **1**, 27–42.
61 G. Obaid, M. Broekgaarden, A. L. Bulin, H. C. Huang, J. Kuriakose, J. Liu and T. Hasan, *Nanoscale*, 2016, **8**, 12471–12503.
62 A. Puri, *Pharmaceutics*, 2013, **6**, 1–25.
63 L. C. Kimlin, G. Casagrande and V. M. Virador, *Mol. Carcinog.*, 2013, **52**, 167–182.
64 L. B. Weiswald, D. Bellet and V. Dangles-Marie, *Neoplasia*, 2015, **17**, 1–15.
65 M. L. Kutys, A. D. Doyle and K. M. Yamada, *Exp. Cell Res.*, 2013, **319**, 2434–2439.
66 C. Evans, *Front. Phys.*, 2015, **3**, DOI: 10.3389/fphy.2015.00015.
67 K. Charoen, B. Fallica, Y. Colson, M. Zaman and M. Grinstaff, *Biomaterials*, 2014, **35**, 2264–2271.
68 U. Till, L. Gibot, P. Vicendo, M. Rols, M. Gaucher, F. Violleau and A. Mingotaud, *RSC Adv.*, 2016, **6**, 69984–69998.
69 D. Hinger, F. Navarro, A. Käch, J. Thomann, F. Mittler, A. Couffin and C. Maake, *J. Nanobiotechnol.*, 2016, **14**, DOI: 10.1186/s12951-016-0221-x.
70 G. Mehta, A. Hsiao, M. Ingram, G. Luker and S. Takayama, *J. Controlled Release*, 2012, **164**, 192–204.
71 D. Herrmann, J. R. Conway, C. Vennin, A. Magenau, W. E. Hughes and J. P. Morton, *Carcinogenesis*, 2014, **35**, 1671–1679.
72 L. E. Fitzpatrick and T. C. McDevitt, *Biomater. Sci.*, 2015, **3**, 12–24.
73 S. Geraldo, A. Simon, N. Elkhatib, D. Louvard, L. Fetler and D. Vignjevic, *Eur. J. Cell Biol.*, 2012, **91**, 63–81.
74 L. Ying and Q. Wang, *BMC Biotechnol.*, 2013, **13**, 76.
75 X. J. Li, A. V. Valadez, P. Zuo and Z. Nie, *Bioanalysis*, 2012, **4**, 1509–1525.
76 S. Halldorsson, E. Lucumi, R. Gomez-Sjoberg and R. M. Fleming, *Biosens. Bioelectron.*, 2015, **63**, 218–231.
77 N. Gupta, J. Liu, B. Patel, D. Solomon, B. Vaidya and V. Gupta, *Bioeng. Transl. Med.*, 2016, **1**, 63–81.
78 E. K. Lumley, C. E. Dyer, N. Pamme and R. W. Boyle, *Org. Lett.*, 2012, **14**, 5724–5727.
79 A. Nyga, U. Cheema and M. Loizidou, *J. Cell Commun. Signal.*, 2011, **5**, 239–248.
80 R. Ng, R. Zang, K. Yang, N. Liu and S. Yang, *RSC Adv.*, 2012, **2**, 10110.
81 V. López-Dávila, H. Welch, M. V. Dwek, I. Uchegbu and M. Loizidou, *Nanomedicine*, 2016, **11**, 331–344.
82 A. Asti and L. Gioglio, *Int. J. Artif. Organs*, 2014, **37**, 187–205.
83 H. Geckil, F. Xu, X. Zhang, S. Moon and U. Demirci, *Nanomedicine*, 2010, **5**, 469–484.
84 J. Zhu and R. E. Marchant, *Expert Rev. Med. Devices*, 2011, **8**, 607–626.
85 U. Cheema, S. Y. Yang, V. Mudera, G. G. Goldspink and R. A. Brown, *Cell Motil. Cytoskeleton*, 2003, **54**, 226–236.
86 R. Brown, M. Wiseman, C. Chuo, U. Cheema and S. Nazhat, *Adv. Funct. Mater.*, 2005, **15**, 1762–1770.
87 M. J. Paszek, N. Zahir, K. R. Johnson, J. N. Lakins, G. I. Rozenberg and A. Gefen, *Cancer Cell*, 2005, **8**, 241–254.
88 K. Ricketts, U. Cheema, A. Nyga, A. Castoldi, C. Guazzoni, T. Magdeldin, M. Emberton, A. Gibson, G. Royle and M. Loizidou, *Small*, 2014, **10**, 3954–3961.
89 B. Dhandayuthapani, Y. Yoshida, T. Maekawa and D. Kumar, *Int. J. Polym. Sci.*, 2011, **2011**, 1–19.
90 R. Perez-Castillejos, *Mater. Today*, 2010, **13**, 32–41.
91 Y. C. Chen, X. Lou, Z. Zhang, P. Ingram and E. Yoon, *Sci. Rep.*, 2015, **5**, 12175.
92 I. Rizvi, J. P. Celli, C. L. Evans, A. O. Abu-Yousif, A. Muzikansky, B. W. Pogue, D. Finkelstein and T. Hasan, *Cancer Res.*, 2010, **70**, 9319–9328.
93 C. L. Evans, A. O. Abu-Yousif, Y. J. Park, O. J. Klein, J. P. Celli, I. Rizvi, X. Zheng and T. Hasan, *PLoS One*, 2011, **6**, 23434.
94 C. J. Rowlands, J. Wu, S. G. Uzel, O. Klein, C. L. Evans and P. T. So, *Laser Phys. Lett.*, 2014, **11**, DOI: 10.1088/612-2011/11/11/115605.
95 I. Rizvi, S. Anbil, N. Alagic, J. Celli, L. Z. Zheng, A. Palanisami, M. D. Glidden, B. W. Pogue and T. Hasan, *Photochem. Photobiol.*, 2013, **89**, 942–952.
96 N. Aggarwal, A. M. Santiago, D. Kessel and B. F. Sloane, *Breast Cancer Res. Treat.*, 2015, **154**, 251–262.

 This journal is © The Royal Society of Chemistry 2018

Open Access Article. Published on 08 2018. Downloaded on 09-08-2025 20:27:54.
This article is licensed under a Creative Commons Attribution 3.0 Unported Licence.

97 A. Martinez de Pinillos Bayona, J. Woodhams, H. Pyea, R. A. Hamoudi, C. M. Moore and A. J. MacRobert, *Cancer Lett.*, 2017, **393**, 68–75.
98 C. O'Rourke, C. Hopper, A. J. MacRobert, J. B. Phillips and J. H. Woodhams, *Int. J. Pharm.*, 2017, **528**, 133–143.
99 K. E. Wright, E. Liniker, M. Loizidou, C. Moore, A. J. Macrobert and J. B. Phillips, *Br. J. Cancer*, 2009, **101**, 658–665.
100 S. Anbil, I. Rizvi, J. P. Celli, N. Alagic, B. W. Pogue and T. Hasan, *J. Biomed. Opt.*, 2013, **18**, 098004.
101 A. Huygens, D. Huyghe, G. Bormans, A. Verbruggen, A. R. Kamuhabwa, T. Roskams and P. A. de Witte, *Photochem. Photobiol.*, 2003, **78**, 607–614.
102 H. Huang, B. Yu, P. Zhang, J. Huang, Y. Chen, G. Gasser, L. Ji and H. Chao, *Angew. Chem., Int. Ed.*, 2015, **54**, 14049–14052.
103 J. Liu, Y. Chen, G. Li, P. Zhang, C. Jin, L. Zeng, L. Ji and H. Chao, *Biomaterials*, 2015, **56**, 140–153.
104 K. Qiu, J. Wang, C. Song, L. Wang, H. Zhu, H. Huang, J. Huang, H. Wang, L. Ji and H. Chao, *ACS Appl Mater Interfaces*, 2017, **9**, 18482–18492.
105 S. S. Lucky, K. C. Soo and Y. Zhang, *Chem. Rev.*, 2015, **115**, 1990–2042.
106 B. Q. Spring, R. B. Sears, L. Z. Zheng, Z. Mai, R. Watanabe, M. E. Sherwood, D. A. Schoenfeld, B. W. Pogue, S. P. Pereira, E. Villa and T. Hasan, *Nat. Nanotechnol.*, 2016, **11**, 378–387.
107 D. K. Chatterjee, L. S. Fong and Y. Zhang, *Adv. Drug Delivery Rev.*, 2008, **60**, 1627–1637.
108 T. T. Wu and S. H. Zhou, *Int. J. Med. Sci.*, 2015, **12**, 187–200.
109 Y. X. Zhu, H. R. Jia, Z. Chen and F. G. Wu, *Nanoscale*, 2017, **9**, 12874–12884.
110 S. Bamrungsap, Z. Zhao, T. Chen, L. Wang, C. Li, T. Fu and W. Tan, *Nanomedicine*, 2012, **7**, 1253–1271.
111 W. Zhang, Y. Li, J. Niu and Y. Chen, *Langmuir*, 2013, **29**, 4647–4651.
112 E. Yaghini, A. M. Seifalian and A. J. MacRobert, *Nanomedicine*, 2009, **4**, 353–363.
113 A. S. Stasheuski, V. A. Galievsky, A. P. Stupak, B. M. Dzhagarov, M. J. Choi, B. H. Chung and J. Y. Jeong, *Photochem. Photobiol.*, 2014, **90**, 997–1003.
114 A. Kamkaew, F. Chen, Y. Zhan, R. Majewski and W. Cai, *ACS Nano*, 2016, **10**, 3918–3935.
115 E. Yaghini, F. Giuntini, I. M. Eggleston, K. Suhling, A. M. Seifalian and A. J. MacRobert, *Small*, 2014, **10**, 782–792.
116 R. Bazak, M. Houri, S. E. Achy, W. Hussein and T. Refaat, *Mol. Clin. Oncol.*, 2014, **2**, 904–908.
117 M. K. Gnanasammandhan, N. M. Idris, A. Bansal, K. Huang and Y. Zhang, *Nat. Protoc.*, 2016, **11**, 688–713.
118 A. Kumari, S. K. Yadav and S. C. Yadav, *Colloids Surf., B*, 2010, **75**, 1–18.
119 A. Mahapatro and D. K. Singh, *J. Nanobiotechnol.*, 2011, **9**, 55.
120 T. Magdeldin, V. Lopez-Davila, J. Pape, G. W. Cameron, M. Emberton, M. Loizidou and U. Cheema, *Sci. Rep.*, 2017, **7**, 44045.
121 Y. Yang, X. Yang, J. Zou, C. Jia, Y. Hu, H. Du and H. Wang, *Lab Chip*, 2015, **15**, 735–744.
122 H. Hung, O. Klein, S. Peterson, S. Rokosh, S. Osseiran, N. Nowell and C. Evans, *Sci. Rep.*, 2016, **6**, 33234.
123 P. Zhang, H. Huang, J. Huang, H. Chen, J. Wang, K. Qiu, D. Zhao, L. Ji and H. Chao, *ACS Appl. Mater. Interfaces.*, 2015, **7**, 23278–23290.
124 J. Liu, K. Liu, L. Feng, Z. Liu and L. Xu, *Biomater. Sci.*, 2017, **5**, 331–340.
125 E. Gaio, D. Scheglmann, E. Reddi and F. Moret, *J. Photochem. Photobiol., B*, 2016, **161**, 244–252.
126 J. Lee, J. Kim, M. Jeong, H. Lee, U. Goh, H. Kim, B. Kim and J. H. Park, *Nano Lett.*, 2015, **15**, 2938–2944.
127 Z. Xiao, C. B. Hansen, T. M. Allen, G. G. Miller and R. B. Moore, *J. Pharm. Pharm. Sci.*, 2005, **8**, 536–543.
128 Y. Wang, Y. Xie, J. Li, Z. H. Peng, Y. Sheinin, J. Zhou and D. Oupicky, *ACS Nano*, 2017, **11**, 2227–2238.
129 M. Benito, V. Martin, M. D. Blanco, J. M. Teijon and C. Gomez, *J. Pharm. Sci.*, 2013, **102**, 2760–2769.
130 J. Zhang, Y. C. Liang, X. Lin, X. Zhu, L. Yan, S. Li, X. Yang, G. Zhu, A. L. Rogach, P. K. N. Yu, P. Shi, L. C. Tu, C. C. Chang, X. Zhang, X. Chen, W. Zhang and C. S. Lee, *ACS Nano*, 2015, **9**, 9741–9756.
131 A. A. Sultan, W. Jerjes, K. Berg, A. Hogset, C. A. Mosse, R. Hamoudi, Z. Hamdoon, Z. Simeon, D. Camell, M. Forster and C. Hopper, *Lancet Oncol.*, 2016, **17**, 1217–1229.
132 A. Martinez de Pinillos Bayona, C. M. Moore, M. Loizidou, A. J. MacRobert and J. H. Woodhams, *Int. J. Cancer*, 2016, **138**, 1049–1057.
133 M. K. Herroon, R. Sharma, E. Rajagurubandara, C. Turro, J. J. Kodanko and I. Podgorski, *Biol. Chem.*, 2016, **397**, 571–582.
134 Y. Shen, A. J. Shuhendler, D. Ye, J. J. Xu and H. Y. Chen, *Chem. Soc. Rev.*, 2016, **45**, 6725–6741.